On the Fragmentation of Ni(II) β-Diketonate- Diamine Complexes as Molecular Precursors for NiO Films: A Theoretical and Experimental Investigation

Cristiano Invernizzi , Gloria Tabacchi * , Roberta Seraglia , Mattia Benedet , Marco Roverso , Chiara Maccato , Sara Bogialli , Davide Barreca * , Ettore Fois

Posted Date: 21 December 2023

doi: 10.20944/preprints202312.1647.v1

Keywords: transition metal complexes; oxide nanomaterials; NiO; molecular precursors; chemical vapor deposition; density functional theory; simulations

Article

On the Fragmentation of Ni(II) β-Diketonate-Diamine Complexes as Molecular Precursors for NiO Films: A Theoretical and Experimental Investigation

Cristiano Invernizzi [1], Gloria Tabacchi [1,*], Roberta Seraglia [2], Mattia Benedet [2,3], Marco Roverso [2,3], Chiara Maccato [2,3], Sara Bogialli [2,3], Davide Barreca [2,*] and Ettore Fois [1]

[1] Department of Science and High Technology - Insubria University and INSTM, 22100 Como, Italy; cinvernizzi@uninsubria.it (C.I.); gloria.tabacchi@uninsubria.it (G.T.); ettore.fois@uninsubria.it (E.F.)
[2] CNR-ICMATE and INSTM, Department of Chemical Sciences, Padova University, 35131 Padova, Italy; roberta.sergalia@cnr.it (R.S.); davide.barreca@unipd.it (D.B.)
[3] Department of Chemical Sciences, Padova University and INSTM, 35131 Padova, Italy; chiara.maccato@unipd.it (C.M.); mattia.benedet@phd.unipd.it (M.B.); marco.roverso@unipd.it (M.R.); sara.bogialli@unipd.it (S.B.)
* Correspondence: gloria.tabacchi@uninsubria.it (G.T.); davide.barreca@unipd.it (D.B.)

Abstract: NiO-based nanomaterials have attracted a great deal of interest in view of various applications, that have stimulated the implementation of various synthetic approaches to control their chemico-physical properties as a function of the desired end-use. In this regard, their bottom-up preparation starting from suitable precursors plays an important role, but a molecular level insight into their reactivity remains an open challenge. In this study, we focus on the fragmentation of Ni(II) diketonate-diamine adducts, of interest as precursors for Ni(II) oxide systems, by combined electrospray ionization mass spectrometry (ESI-MS) with multiple collisional experiments ($ESI\text{-}MS^n$) and theoretical calculations. The joint analyses revealed common features in the fragmentation pattern of the target compounds: i) in the first-fragmentation, all three complexes form analogous base-peak cations by losing a negatively charged diketonate; in these cations, Ni-O and Ni-N interactions are stronger and the Ni positive charge is lower than in the neutral complexes; ii) the tendency of ligand electronic charge to migrate towards Ni further increases in the subsequent fragmentation processes, leading to the formation – in all three cases – of a tetracoordinated Ni environment involving an interesting cation-π intramolecular interaction.

Keywords: transition metal complexes; oxide nanomaterials; NiO; molecular precursors; chemical vapor deposition; density functional theory; simulations.

1. Introduction

Nanomaterials based on NiO, a multi-functional *p*-type semiconductor, have been the object of numerous studies thanks to their scientific and technological interest in view of various end-uses, among which electrochromic devices [1], solar cells [2], and heterogeneous catalysts for a variety of processes [3–8]. This wide perspective of utilization has boosted the interest in their preparation by bottom-up approaches, among which sol-gel and chemical vapor deposition (CVD) [9–11], that are endowed with several degrees of freedom to tailor material structure, chemical composition and morphology already during their preparation. In particular, the CVD family encompasses a variety of routes based on heterogeneous nucleation and growth processes, deeply influenced by the nature and features of the starting molecular compounds [12–14].

In this context, metal β-diketonate complexes are among the most widely used precursors for the CVD of metal oxide films and nanomaterials [15,16]. They offer a significant flexibility in the modification of their chemical and physical properties by varying the steric hindrance, size and features of the ligand backbone [15]. Nevertheless, as regards the CVD of NiO, the conventional $[Ni(acac)_2]$ [7,17] and $[Ni(thd)_2]$ [18,19] (Hacac = 2,4-pentanedione; Hthd = 2,2,6,6-tetramethyl-3,5-

 doi:10.20944/preprints202312.1647.v1

heptanedionate) suffer from a variety of problems, including the high melting points and the limited gas phase stability [15,17,20–22], that hinder the possibility of attaining a precise process control and precludes their straightforward large-scale use.

As a valuable alternative, following our previous works on homologous first-row transition metal compounds [12,13,23–31], we have focused on the synthesis and characterization of Ni(II) β-diketonate-diamine adducts of general formula NiL_2TMEDA [HL = 1,1,1,-trifluoro-2,4-pentanedionate (tfa), 2,2-dimethyl-6,6,7,7,8,8,8-heptafluoro-3,5-octanedionate (fod), or thd; TMEDA = N,N,N′,N′-tetramethylethylenediamine]. The combined results of a comprehensive theoretical and experimental investigation [32,33] highlighted that this compound family offers a set of amenable characteristics for applications as CVD precursors of NiO films with modular properties. Information on the compound reactivity was obtained by electron ionization mass spectrometry (EI-MS), whose hard ionization conditions lead to the destruction of specific diagnostic ions due to the fragmentation of the intact complex [13]. Complementary information are achievable by soft ionization methods like electrospray ionization-mass spectrometry (ESI-MS) [23,24,26].

In this work, fragmentation behaviors of three compounds, i.e. $Ni(tfa)_2TMEDA$ (**1**), $Ni(fod)_2TMEDA$ (**2**) and $Ni(thd)_2TMEDA$ (**3**), were analyzed both experimentally and theoretically. We specifically focus on the fragmentation of NiL_2TMEDA, investigated by electrospray ionization-high resolution mass spectrometry (ESI-HRMS), $ESI\text{-}MS^n$ experiments, and theoretical investigations. A detailed computational study based on density functional theory (DFT) calculations was carried out, with the aim of elucidating the molecular structure of NiL_2TMEDA fragments. This information is also complemented by a thorough investigation on the electronic structure of the latter, which reveals how the metal-ligands bonding scheme evolves in passing - *via* the loss of specific ligands - from the full precursor to the fragments identified from mass spectra. Overall, the obtained outcomes provide for the first time a valuable insight into the gas-phase fragmentation mechanisms of such compounds as a function of the ligand nature, as well as a detailed insight on both geometric and electronic structure of the fragmentation products, setting the basis for a molecular-level understanding of their reactivity.

2. Results

2.1. ESI-MS Experiments

Positive ion mode ESI-HRMS mass spectra for the three complexes are reported in Figure 1, whereas the identification of the main fragments, m/z ratios, and relative abundances are given in Table 1. In all spectra, the base peak was due to the loss of a β-diketonate ligand L, leading to the more stable $[M\text{-}L]^+$ species (m/z = 327.0830, 469.1229 and 357.2041 for **1**, **2** and **3**, respectively). Ions due to the protonated diamine $[TMEDA+H]^+$ are detected at m/z = 117.1390 with a relative abundance higher than 45% for all complexes. Only for **2**, the molecular ion was detected as sodium adduct at m/z = 787.1690 ($[M+Na]^+$), together with those at m/z = 671.0379 due to TMEDA loss ($[M\text{-}TMEDA+Na]^+$). The presence of $[M+Na]^+$ for **2** can be attributed to a good efficiency in the formation of Na adducts under ESI-MS conditions by fluorine atoms of $CF_2CF_2CF_3$ groups, due to their partial negative charge [34]. For compound **3** the ion at m/z 425.2190 is attributable to the loss of TMEDA from protonated molecular ion (not detectable). For compound **1**, intact molecular ions, both protonated or cationized, are not present. MS/MS experiments (see Figure 2) on $[M\text{-}L]^+$ ions revealed further decomposition processes due to TMEDA-related rearrangements. In particular, the loss of $NH(CH_3)_2$ from TMEDA moiety turned out to be the most favored fragmentation process, resulting in the formation of ions at m/z = 282, 424 and 312 for **1**, **2** and **3**, respectively. In addition, for fluorinated compounds **1** and **2**, the loss of $-CH_3CH_2N(CH_3)_2$ from $[M\text{-}L]^+$ led to ionic species at m/z = 254 and 396, respectively. Only for $[M\text{-}L]^+$ of compound **2**, an additional rearrangement of fod ligand was present at m/z = 413, due to $C(CH_3)_2{=}CH_2$ loss.

Preprints (www.preprints.org) | NOT PEER-REVIEWED | Posted: 21 December 2023 doi:10.20944/preprints202312.1647.v1

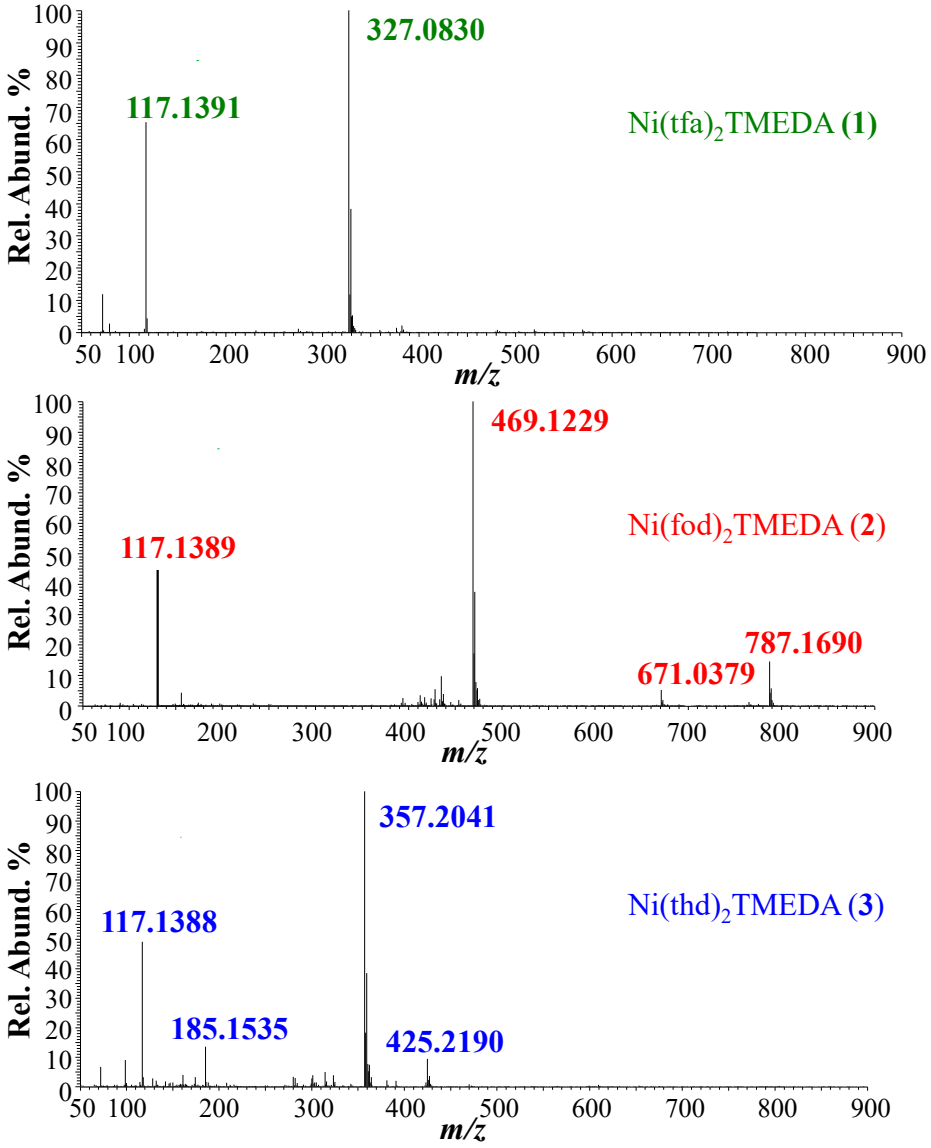

Figure 1. Positive ESI-HRMS spectra of methanolic solution of compounds **1**-**3**.

Table 1. Selected fragments, *m*/*z* ratios, and relative abundances (%) obtained in ESI-HRMS analyses of compounds **1**, **2**, and **3**.

	1	2	3
Ionic species	***m*/*z* (%)**	***m*/*z* (%)**	***m*/*z* (%)**
$[M+Na]^+$	---	787.1690 (25)	---
$[M-TMEDA+Na]^+$	---	671.0379 (12)	---
$[M-TMEDA+H]^+$	---	---	425.2190 (15)
$[M-L]^+$	327.0830 (100)	469.1229 (100)	357.2041 (100)
$[HL+H]^+$	---	---	185.1535 818)
$[TMEDA+H]^+$	117.1391 (70)	117.1389 (50)	117.1388 (55)

Preprints (www.preprints.org) | NOT PEER-REVIEWED | Posted: 21 December 2023 doi:10.20944/preprints202312.1647.v1

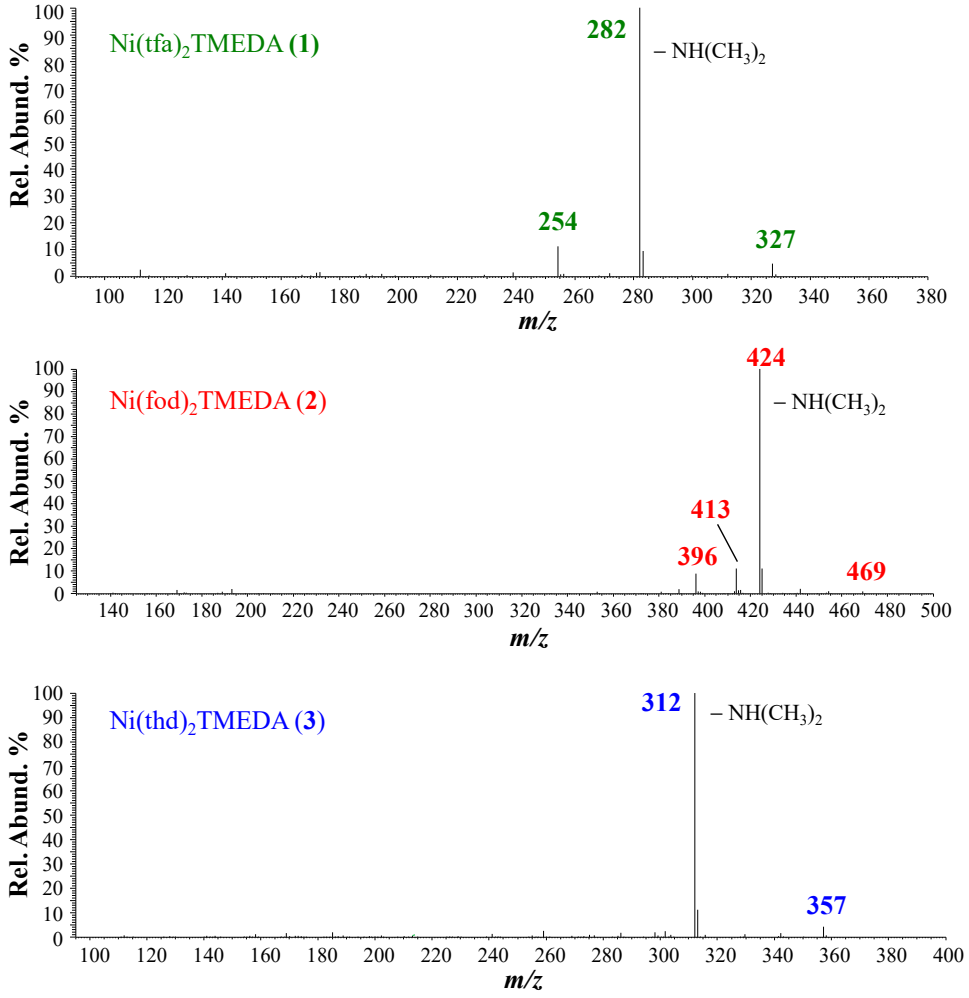

Figure 2. ESI-MS^2 spectra of $[M-L]^+$ ions for compounds **1**, **2**, and **3**.

2.2. DFT Calculations

In order to elucidate the molecular structures of fragment ions detected in mass spectrometry experiments, a series of DFT calculations has been performed, starting from the computation of the minimum energy structures of the three neutral complexes [Ni(L)$_2$TMEDA] (Figure 3). Additionally, all fragments discussed in the previous section have been subjected to structural optimizations. The resulting optimized geometries are depicted in Figures 3, 4, S1 and S2, while relevant geometrical parameters are reported in Tables 2, 4 and S1.

A graphical representation of the optimized structures of the neutral complexes obtained for L= tfa, fod, and thd is shown in Figure 3a,c,e, respectively. Since all ESI-HRMS spectra showed a base peak due to the loss of a β-diketonate ligand L, a search for the minimum energy structures of $[M-L]^+$ species has been performed starting from the optimized structures of neutral complexes and removing a β-diketonate ligand. The resulting optimized geometries of $[Ni(L)TMEDA]^+$ with L = tfa, fod, and thd are depicted in Figure 3b,d,f, respectively.

Preprints (www.preprints.org) | NOT PEER-REVIEWED | Posted: 21 December 2023 doi:10.20944/preprints202312.1647.v1

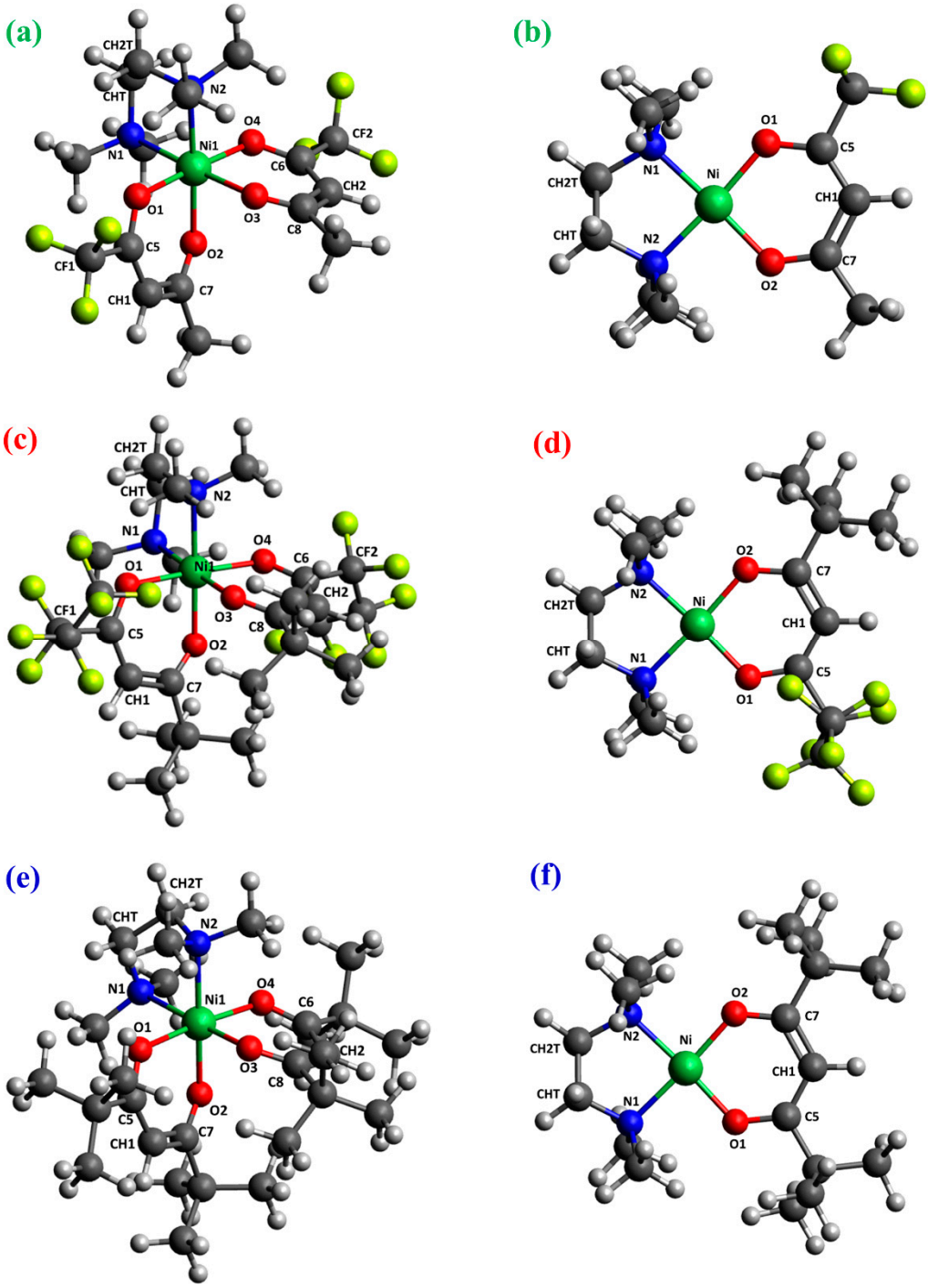

Figure 3. DFT-computed minimum energy structures for [Ni(L)$_2$TMEDA] with L = tfa (a), fod (c), thd (e), and for [Ni(L)TMEDA]$^+$ with L = tfa (b), fod (d), and thd (f).Color codes: green = Ni; yellow = F; blue = N; red = O; grey = C; white = H.

Preprints (www.preprints.org) | NOT PEER-REVIEWED | Posted: 21 December 2023 doi:10.20944/preprints202312.1647.v1

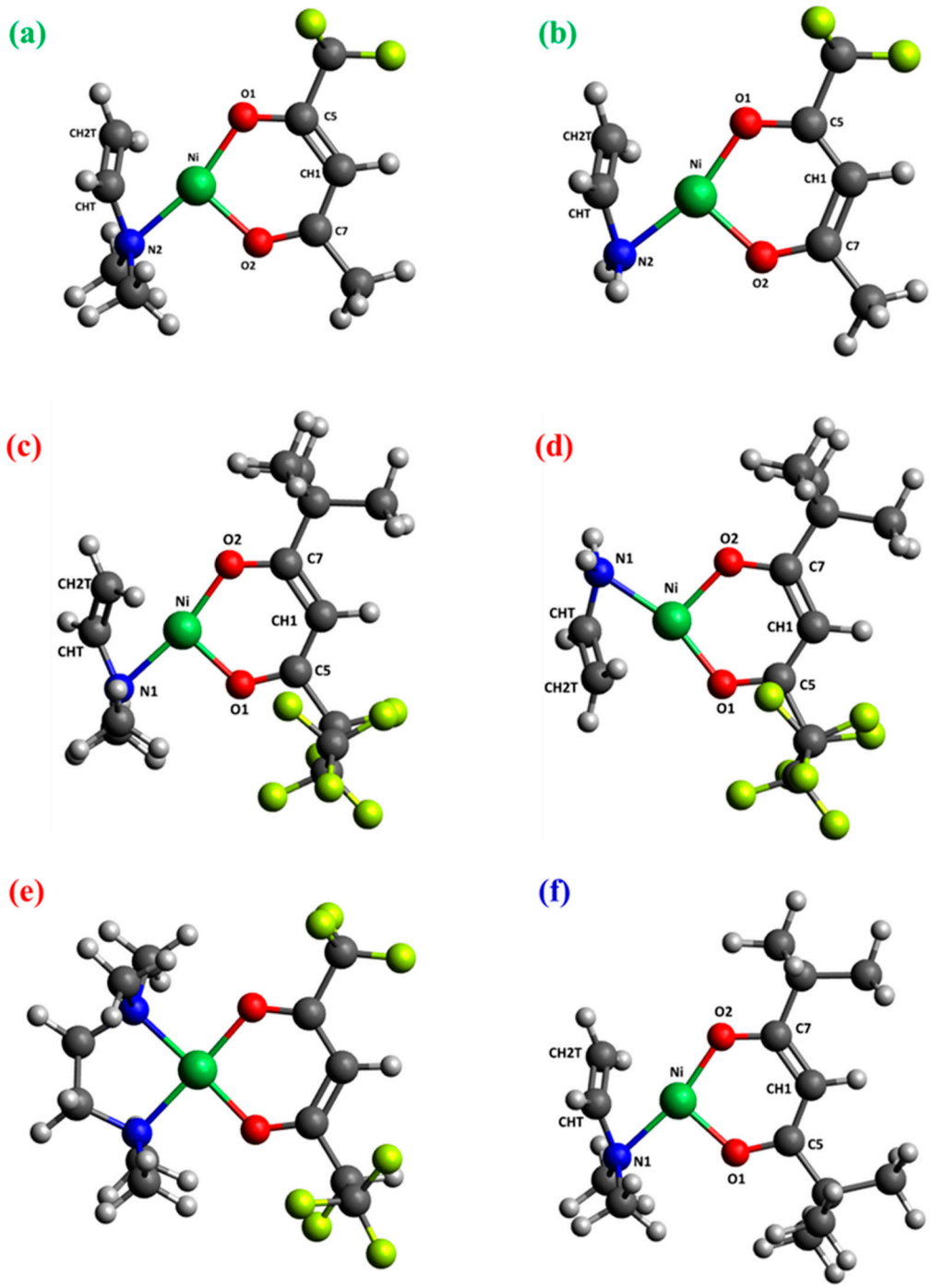

Figure 4. Graphical representation of the optimized structures of: (a) [Ni(tfa)TMEDA]$^+$-$NH(CH_3)_2$; (b) [Ni(tfa)TMEDA]$^+$-$CH_3CH_2N(CH_3)_2$; (c) [Ni(fod)TMEDA]$^+$-$NH(CH_3)_2$; (d) [Ni(fod)TMEDA]$^+$-$CH_3CH_2N(CH_3)_2$; (e) [Ni(fod)TMEDA]$^+$-$(CH_3)_2C{=}CH_2$, due to an additional rearrangement of fod ligand; (f) [Ni(thd)TMEDA]$^+$-$NH(CH_3)_2$. Color codes: green = Ni; yellow = F; blue = N; red = O; grey = C; white = H.

As far as the neutral complexes are concerned, their molecular geometries are similar among each other and close to the structural parameters computed with another density functional approximation [32]. In particular, in all the three neutral complexes Ni exhibits a slightly distorted octahedral coordination environment, characterized by Ni-O distances shorter than Ni-N ones (see Table 2), suggesting that the interactions between metal center and oxygen atoms should be stronger than those with nitrogen ones. This hypothesis is substantiated by the bond order (BO) trend, as the

Preprints (www.preprints.org) | NOT PEER-REVIEWED | Posted: 21 December 2023 doi:10.20944/preprints202312.1647.v1

Ni-O BOs are systematically higher than the Ni-N ones for all three compounds (see Table 2). Interestingly, whereas BO values for Ni-O bonds are quite similar among the three complexes, the Ni-N bond order for the non-fluorinated compound **3** - bearing two tert-butyl group *per* diketonate ligand - is slightly lower than that found for fluorinated complexes **1** and **2**. These data indicate that, whereas F-containing groups cope to increase the Ni-N bond strength, the presence of tert-butyl substituents has the opposite effect – *i.e.*, weakening Ni-N interactions. Nonetheless, beside these slight differences, both the molecular geometry and the electronic structure underlying the metal-ligand bonding scheme show a strong similarity in the three compounds, as evidenced by Figure 3 and the data in Table 2. This result might rationalize the similar fragmentation behavior of the target complexes as deduced from Figure 1, in particular the presence of $[M-L]^+$ as the base peak in all ESI-HRMS spectra.

Table 2. Selected bond lengths (BL) (in Å), and corresponding bond orders (BO) from the optimized structures of neutral complexes M and fragments $[M-L]^+$ for compounds **1**, **2**, and **3**. Different colors in the BO columns refer to different ligands (brown and violet = first and second diketonate ligand, respectively; gray = TMEDA). Atom labels as in Figure 3.

	1				**2**				**3**			
	M		**[M-tfa]⁺**		**M**		**[M-fod]⁺**		**M**		**[M-thd]⁺**	
	BL	*BO*	*BL*	*BO*	*BL*	*BO*	*BL*	*BO*	*BL*	*BO*	*BL*	*BO*
Ni-O1	2.024	0.284	1.831	0.471	2.035	0.242	1.833	0.454	2.018	0.241	1.828	0.476
Ni-O4	2.024	0.284			2.035	0.242			2.018	0.241		
Ni-O2	2.041	0.294	1.848	0.469	2.023	0.258	1.842	0.452	2.009	0.256	1.828	0.476
Ni-O3	2.041	0.294			2.023	0.258			2.010	0.256		
Ni-N1	2.147	0.230	1.946	0.405	2.153	0.201	1.946	0.393	2.165	0.178	1.957	0.368
Ni-N2	2.147	0.230	1.946	0.399	2.153	0.201	1.947	0.387	2.165	0.178	1.957	0.368
O1-C5	1.260	1.362	1.276	1.285	1.260	1.363	1.276	1.279	1.267	1.352	1.284	1.267
O2-C7	1.257	1.427	1.274	1.318	1.258	1.418	1.276	1.316	1.263	1.376	1.284	1.267
O4-C6	1.260	1.362			1.260	1.363			1.267	1.352		
O3-C8	1.257	1.427			1.258	1.418			1.263	1.376		
C5-CH1	1.392	1.423	1.380	1.450	1.393	1.421	1.381	1.451	1.411	1.348	1.400	1.367
C7-CH1	1.424	1.264	1.413	1.300	1.425	1.260	1.413	1.288	1.414	1.325	1.400	1.367
C6-CH2	1.392	1.423			1.393	1.421			1.411	1.348		
C8-CH2	1.424	1.264			1.425	1.260			1.414	1.325		
CHT-CH2T	1.520	1.021	1.508	1.027	1.518	1.021	1.507	1.027	1.520	1.020	1.508	1.026

Indeed, similar considerations hold for the minimum energy structures calculated for $[M-L]^+$ fragments, all characterized by very similar geometric arrangements and metal-ligand bonding schemes. Specifically, as illustrated by Figure 3b,d,f, all three ions are characterized by a square-planar geometry, typical of tetra-coordinated Ni(II) complexes in the singlet spin state. Moreover, data in Table 2 indicate that both geometrical parameters and BOs values show only very slight differences in passing from compound **1** to **2** to **3**. This finding is further supported by the Natural Bond Orbital (NBO) analysis performed on the electronic structure of the three $[M-L]^+$ fragments. In particular, the data reported in Table S2 indicate a very strong similarity of the NBOs localized on the metal-ligand bonds. Irrespective of the diketonate nature, all NBOs have σ-character. While the bonding components (BD(σ)) are mostly localized on ligand's nitrogen and oxygen atoms (≈90%), the antibonding components (BD(σ*)) are predominantly localized on Ni. Taken together, NBO data indicate that electron charge is transferred by the ligands towards Ni. This finding is further clarified by the graphical representation of the aforementioned bonding NBO's - depicted in Figures S3, S4, and S5 for L = tfa, fod, and thd, respectively –, highlighting the net σ-character of the orbital, as well as Ni participation to the bonding scheme. Such a close similarity in the electronic structure might

Preprints (www.preprints.org) | NOT PEER-REVIEWED | Posted: 21 December 2023 doi:10.20944/preprints202312.1647.v1

suggest that all three ions are characterized by a similar stability and may all easily form in ESI-HRMS conditions.

Notably, for all the target complexes, Ni-O and Ni-N distances undergo a significant shortening upon passing from neutral compounds to $[M-L]^+$ fragments. This trend is paralleled by the considerable increase of the corresponding bond orders, which are nearly doubled in the fragment ions. Hence, in terms of the metal-ligand bonding, the loss of a diketonate ligand results in a significant strengthening of Ni-TMEDA interactions and of Ni-O bonds of the remaining diketonate moiety.

A useful feature of NBO analysis is the opportunity of partitioning the electronic density between 'subsystems' – *i.e.*, specific portions of a given molecule, allowing thus to estimate the total charge on each subsystem. In this case, it is particularly instructive to inspect the total NBO charges localized on Ni, diketonate ligand L, and TMEDA, reported in Table 3. Interestingly, the data show that the positive charge on Ni decreases by ≈ 25-30% on passing from neutral complex to $[M-L]^+$ cations. This result, that may appear counterintuitive given the fragments' positive charge, may be explained by considering that the donation of electronic charge from both L and TMEDA to Ni increases significantly upon the loss of a diketonate ligand. Indeed, the total negative charge on L decreases by 50%, whereas the total (positive) charge on TMEDA is more than doubled (Table 3). Hence, these data clearly indicate that all $[M-L]^+$ species are stabilized by a strong donation of electronic density from the ligands towards the metal center. This effect is slightly stronger in the fragment derived from compound **3**, due to the higher electron-donor character of the two tert-butyl substituents on the diketonate moiety with respect to fluorine-containing groups, present in compounds **1-2**.

Table 3. NBO charges on Ni, diketonate ligand L, and on TMEDA computed for the optimized structures of neutral complexes M and fragments $[M-L]^+$ for compounds **1**, **2**, and **3**. Different colors refer to different ligands (brown = diketonates, gray = TMEDA).

	1		**2**		**3**	
	M	**$[M-tfa]^+$**	**M**	**$[M-fod]^+$**	**M**	**$[M-thd]^+$**
Ni	1.00	0.73	1.08	0.75	1.12	0.75
L	-0.65	-0.35	-0.68	-0.36	-0.69	-0.32
TMEDA	0.30	0.62	0.28	0.61	0.26	0.57

Beside the main peak, which is common to the three complexes, ESI-HRMS spectra indicated the formation of other cations (see Figure 1 and Table 1). A careful computational search of the minimum energy structure of these species has been performed as well. Graphical representations of optimized geometries of $[M+Na]^+$, $[M-TMEDA+Na]^+$, $[M-TMEDA+H]^+$, $[HL+H]^+$ and $[TMEDA+H]^+$ are shown in Figure S1, while selected geometrical parameters are reported in Table S1. It should be pointed out that Na^+ is present only in ESI-HRMS spectra of the fluorine-richest compound **2**. In $[M+Na]^+$, Ni maintains its octahedral environment in spite of the entrance of Na^+ in the second coordination shell (Figure S1a). Specifically, three O atoms appear to be at coordination distances from Na (average Na-O distance = 2.416 Å), which is also interacting with a fluorine atom (Na-F distance = 2.441 Å). The consequent distortion of the octahedral Ni environment is evidenced by the lengthening of Ni-O and Ni-N bonds with respect to the neutral complex $[Ni(fod)_2TMEDA]$. This effect is particularly relevant for the bonds involving the three oxygen atoms also coordinated with Na^+ (Table S1). Similarly, the species $[M-TMEDA+Na]^+$ - exhibiting a distorted square-planar Ni coordination geometry, is characterized by significant O-Na^+ and F-Na+ interactions (Table S1, Figure S1b). In a different way, the $[M-TMEDA+H]^+$ species - namely $[Ni(thd)_2+H]^+$ - is protonated at the CH1 carbon. For this ion, two structures very close in energy (ΔE = 0.32 kcal/mol) have been found (Figure S1c,d). The most stable one exhibits a distorted tetrahedral arrangement around the Ni center, and has triplet spin multiplicity, whereas the less stable one shows a distorted square planar arrangement and singlet spin multiplicity. Given the modest energy difference, both structures might be formed during the ESI process. The presence of the protonated diketonate species $[HL+H]^+$ has been detected only for

the case of the more electron-donor thd ligand. Its optimized structure is characterized by the protonation of both carbonylic groups (Figure S1e). On the other hand, the other protonated ligand $[TMEDA+H]^+$ is detected in the fragmentation of all three complexes. In this case, the protonation occurs on one of the nitrogen atoms (see Figure S1f).

As far as MS^2 spectra are concerned, attention was focused on the subsequent fragmentation of $[M-L]^+$ cations. Even in this case, the spectra of the three cations presented common features, in particular the formation of $[M-L]^+$ - $NH(CH_3)_2$ species. The theoretical search of the minimum energy structure of these moieties led to the molecular geometries depicted in Figure 4a,c,f for L = tfa, fod, thd, respectively. Remarkably, these cations have very similar geometries and Ni-ligands bonding patterns. Whereas the diketonate remains coordinated to Ni with both its oxygen atoms, only one nitrogen atom (the one survived to the fragmentation) is linked to the metal center. Nevertheless, Ni maintains its nearly square-planar coordination geometry thanks to the interaction with a double C=C bond formed upon - $NH(CH_3)_2$ release. Specifically, the Ni-CHT and Ni-CH2T distances become ≈ 2 Å in these fragments (see Table 4). Moreover, data in Table 4 clearly indicate a net shortening of CHT-CH2T bond length (Figure 4) compared to the same distance in $[M-L]^+$ species (Table 2). This distance shortening is accompanied by a significant increase of the CHT-CH2T bond order (from values of ≈ 1 to values greater than 1.5, see Tables 2 and 4). Correspondingly, Ni-CHT and Ni-CH2T BOs values become comparable to those of Ni-O/Ni-N bonds, indicating appreciable Ni-C interactions which are greater for the terminal C atom (CH2T), closer to Ni. These observations are common to the three cations, underlining once again the similarity of the metal-ligand bonding scheme among systems derived from compounds **1**, **2**, **3**.

The loss of a $-CH_3CH_2N(CH_3)_2$ group is detected only for the fluorinated $[M-L]^+$ species derived from complexes **1** and **2**. In these cations (see Figure 4 b,d), the bonding pattern around Ni is practically the same as in $[M-L]^+$ - $NH(CH_3)_2$ species, discussed previously. The planar tetra-coordinated Ni structure is characterized by two Ni-O bonds, one Ni-N bond and a cation-π intramolecular interaction between the Ni center and the CHT=CH2T double bond. Figures S6-S10 report a graphical representation of the relevant orbitals involved in this cation-π interaction, whereas Tables S3 and S4 report the quantitative NBO analysis. As can be seen from both orbital representations and NBO analysis, Ni cation actively participates to such an interaction, with the π structure predominantly localized on the CHT=CH2T double bond.

Concerning complex **2**, species corresponding to the loss of a $CH_3C=CH_2$ group from $[Ni(fod)TMEDA]^+$ have been detected ($[Ni(fod)TMEDA]^+$-$(CH_3)_2C=CH_2$) in ESI-MS spectra. Their stoichiometry indicates a rearrangement of the fod ligand (see Figure 1 and Table 1). In order to identify the structure of these cations, geometry optimizations have been performed on different hypothetical guess structures characterized by such a stoichiometry. Figure S2 contains a graphical representation of the six most stable structures, along with their relative stability (including the zero-point contribution). The most stable structure (Figure S2a) is characterized by a distribution of fluorine atoms on both diketonate ligand sides. A similar feature is also present in the other lower energy isomers.

Finally, the trend of the Bader charges on passing form the neutral complex to the positive ions further evidences common features in the fragmentation of the three complexes (see Tables S5-S8). Indeed, it is possible to deduce a displacement of electrons from ligands to the metal center, whose positive charge is significantly depleted along the fragmentation. This finding is also in line with the arguments deduced from NBO analysis. Notably, such an electron-enrichment tendency of the metal center during $[Ni(L)_2TMEDA]$ precursors' fragmentation might be relevant for CVD processes, where an electron-richer Ni cation (nearly +1) could be more prone to be oxidized by the molecular oxygen present in the reaction atmosphere, facilitating thus the formation of NiO films.

Preprints (www.preprints.org) | NOT PEER-REVIEWED | Posted: 21 December 2023 doi:10.20944/preprints202312.1647.v1

Table 4. Selected bond lengths (BL) (in Å) and corresponding bond orders (BO) from the optimized structures of fragments detected in ESI-MS² spectra of $[M-L]^+$ ions for compounds **1**, **2**, and **3**. Different colors in the BO columns refer to different ligands (brown = diketonate, gray = TMEDA). Atom labels as in Figure 4.

	1				2						3	
	$[M-tfa]^+$-$NH(CH_3)_2$		$[M-tfa]^+$-$CH_3CH_2N(CH_3)_2$		$[M-fod]^+$-$NH(CH_3)_2$		$[M-fod]^+$-$CH_3CH_2N(CH_3)_2$		$[M-fod]^+$-$(CH_3)_2C=CH_2$		$[M-thd]^+$-$NH(CH_3)_2$	
	BL	*BO*	*BL*	*BO*	*BL*	*BO*	*BL*	*BO*	*BL*	*BO*	*BL*	*BO*
Ni-O1	1.811	0.523	1.799	0.557	1.814	0.506	1.794	0.554	1.837	0.450	1.808	0.535
Ni-O2	1.830	0.511	1.819	0.541	1.816	0.518	1.815	0.543	1.842	0.453	1.803	0.546
Ni-N1	-		-		1.929	0.391	1.946	0.402	1.938	0.415	1.941	0.368
Ni-N2	1.932	0.393	1.943	0.408					1.937	0.414		
Ni-CHT	1.972	0.248	1.987	0.264	1.976	0.239	1.986	0.264			1.974	0.243
Ni-CH2T	2.096	0.394	2.128	0.368	2.098	0.393	2.128	0.363			2.108	0.375
O1-C5	1.277	1.288	1.281	1.267	1.280	1.258	1.281	1.263	1.265	1.342	1.288	1.264
O2-C7	1.281	1.297	1.279	1.308	1.279	1.314	1.280	1.299	1.270	1.318	1.287	1.264
C5-CH1	1.384	1.444	1.381	1.463	1.380	1.468	1.381	1.458	1.400	1.345	1.399	1.381
C7-CH1	1.409	1.315	1.412	1.300	1.417	1.281	1.413	1.292	1.389	1.404	1.403	1.361
CHT-CH2T	1.379	1.566	1.373	1.588	1.380	1.567	1.373	1.590	1.508	1.027	1.378	1.579

3. Materials and Methods

3.1. Experimental Details

$Ni(L)_2TMEDA$ complexes (with L=tfa, fod, thd) were synthesized following recently reported procedures [32]. Electrospray ionization-high resolution mass spectrometric (ESI-HRMS) data were acquired by a Q Exactive™ hybrid quadrupole-Orbitrap™ mass spectrometer (ThermoFisher Scientific) in positive ion mode (resolution = 70000; sheath gas N_2 at 10 psi; spray voltage = 3.5 kV and capillary temperature 280°C). Orbitrap MS calibration was performed using a standard ThermoFisher Scientific Pierce® ESI positive ion calibration solution). 10^{-6} M solutions of the target compounds were introduced by direct infusion using a syringe pump (flow rate = 10 $\mu L \times min^{-1}$). Low resolution electrospray ionization-mass spectrometry (ESI-MS) analyses were performed using a LCQFleet ion trap instrument (ThermoFisher Scientific), operating in positive ion mode. The used spray voltage and capillary temperature were 4.0 kV and 250°C, respectively. 10^{-6} M solutions of the target compounds were introduced by direct infusion using a syringe pump (flow rate = 10 $\mu L \times min^{-1}$). MS experiments were performed by applying a supplementary Radio Frequency (RF) voltage to the end caps of the ion trap (5 V peak-to-peak).

 doi:10.20944/preprints202312.1647.v1

3.2. Computational Details

Density functional theory calculations were performed on the target compounds [Ni(L)$_2$TMEDA] (with L=tfa, fod, thd) and their fragments. Specifically, the M06 functional [35] was adopted using the Gaussian 09 code [36]. The choice of this density functional approximation was suggested by its capability of delivering a good description of molecular and electronic structure of transition metal compounds – in particular ionic species, as evidenced in the study of fragmentation of a similar Cu(II) complex - namely [Cu(hfa)$_2$TMEDA] [30]. For Ni, an "energy-adjusted" ab initio pseudopotential and (8s7p6d2f1g)/[6s5p3d2f1g] basis set were employed [37]. For all the other atoms, the D95(d) basis set has been adopted, except for Na, for which the 6-31G(d) set was employed [38]. All the computed optimized structures were characterized by no imaginary frequencies. Zero-point-energy (ZPE) correction was taken into account in all the reported energy differences.

Bonding properties were theoretically investigated via the Natural Bond Orbitals analysis (NBO) [39]. Atomic charges were obtained adopting the Bader approach [40,41]. Both NBO analysis and Bader charges were calculated using the same level of theory of the structural optimizations.

4. Conclusions

The chemical reactivity of three Ni(L)$_2$TMEDA complexes (L=tfa, fod and thd ligand, respectively) in decomposition processes was explored by adopting soft fragmentation procedures and via computational models. The combined experimental and theoretical analyses, besides some ligand-dependent features, evidenced relevant common elements in the fragmentation pattern of the target compounds: i) in cations formed in the first fragmentation, Ni-O and Ni-N interactions are stronger and the positive charge on Ni is lower than in neutral complexes; ii) the tendency of ligand electronic charge to migrate progressively towards Ni further increases in the subsequent fragmentation processes, leading to the formation – in all three cases – of a tetracoordinated Ni environment involving C atoms belonging to partially fragmented TMEDA. From both the structural and electronic point of view, it is also interesting to notice the formation of a C-C double bond in TMEDA rearrangements. As evidenced by the NBO analysis, such a double bond – as substantiated by the bond order trend - is actually interacting with the Ni cation via an intramolecular cation-π interaction. In perspective, these analyses can be relevant in view of the application of these compounds in CVD processes.

Supplementary Materials: The following supporting information can be downloaded at the website of this paper posted on Preprints.org. The supporting material file contains the graphical representations of minimum energy structures relevant for the fragmentation processes (Figures S1 and S2). Graphical representations of relevant Natural Bond Orbitals for diverse fragments (Figures S3 to S10). Tables relative to relevant geometrical parameters and NBO analyses of fragments discussed in the main text (Tables S1 to S4). Tables containing the atomic charges obtained via the Bader analysis (Tables S5 to S8).

Author Contributions: Conceptualization, C.I., G.T., E.F. and D.B.; writing—original draft preparation, G.T., M.B. and C.M.; investigation, R.S., M.R., S.B..; data curation, C.I. and G.T.; formal analysis, C.I., E.F., G.T.; validation, R.S., M.R., S.B.; project administration, D.B., C.M., E.F., G.T.; visualization, E.F., C.I, G.T..; funding acquisition, D.B., E.F., G.T., C.M.; writing—reviewing and editing, all authors. All authors have read and agreed to the published version of the manuscript.

Funding: This research was funded by CNR (Progetti di Ricerca @CNR - avviso 2020 - ASSIST), Padova University (PDiSC#04BIRD2020-UNIPD EUREKA, DOR 2021–2023), INSTM Consortium (INSTM21PDBARMAC-ATENA), and Insubria University (FAR2021).

Data Availability Statement: Data is contained within the article or supplementary material.

Acknowledgments: Thanks are due to Dr. D. Canton for technical support.

Conflicts of Interest: The authors declare no conflict of interests. The funders had no role in the design of the study; in the collection, analyses, or interpretation of data; in the writing of the manuscript, or in the decision to publish the results.

Sample Availability: Samples of the compounds Ni(L)$_2$TMEDA (with L=tfa, fod, thd) are available from the

authors.

References

1. Sialvi, M.Z.; Mortimer, R.J.; Wilcox, G.D.; Teridi, A.M.; Varley, T.S.; Wijayantha, K.G.U.; Kirk, C.A. Electrochromic and colorimetric properties of nickel(II) oxide thin films prepared by aerosol-assisted chemical vapor deposition. *ACS Appl. Mater. Interfaces* **2013**, *5*, 5675-5682, doi:10.1021/am401025v.
2. Wilson, R.L.; Macdonald, T.J.; Lin, C.-T.; Xu, S.; Taylor, A.; Knapp, C.E.; Guldin, S.; McLachlan, M.A.; Carmalt, C.J.; Blackman, C.S. Chemical vapour deposition (CVD) of nickel oxide using the novel nickel dialkylaminoalkoxide precursor [Ni(dmamp')$_2$] (dmamp' = 2-dimethylamino-2-methyl-1-propanolate). *RSC Adv.* **2021**, *11*, 22199-22205, doi:10.1039/D1RA03263A.
3. Han, S.W.; Kim, I.H.; Kim, D.H.; Park, K.J.; Park, E.J.; Jeong, M.-G.; Kim, Y.D. Temperature regulated-chemical vapor deposition for incorporating NiO nanoparticles into mesoporous media. *Appl. Surf. Sci.* **2016**, *385*, 597-604, doi:10.1016/j.apsusc.2016.05.160.
4. Kitchamsetti, N.; Ramteke, M.S.; Rondiya, S.R.; Mulani, S.R.; Patil, M.S.; Cross, R.W.; Dzade, N.Y.; Devan, R.S. DFT and experimental investigations on the photocatalytic activities of NiO nanobelts for removal of organic pollutants. *J. Alloys Compd.* **2021**, *855*, 157337, doi:10.1016/j.jallcom.2020.157337.
5. Zywitzki, D.; Taffa, D.H.; Lamkowski, L.; Winter, M.; Rogalla, D.; Wark, M.; Devi, A. Tuning coordination geometry of nickel ketoiminates and its influence on thermal characteristics for chemical vapor deposition of nanostructured NiO electrocatalysts. *Inorg. Chem.* **2020**, *59*, 10059-10070, doi:10.1021/acs.inorgchem.0c01204.
6. An, W.-J.; Thimsen, E.; Biswas, P. Aerosol-chemical vapor deposition method for synthesis of nanostructured metal oxide thin films with controlled morphology. *J. Phys. Chem. Lett.* **2010**, *1*, 249-253, doi:10.1021/jz900156d.
7. Weidler, N.; Schuch, J.; Knaus, F.; Stenner, P.; Hoch, S.; Maljusch, A.; Schäfer, R.; Kaiser, B.; Jaegermann, W. X-ray photoelectron spectroscopic investigation of plasma-enhanced chemical vapor deposited NiO_x, $NiO_x(OH)_y$, and $CoNiO_x(OH)_y$: influence of the chemical composition on the catalytic activity for the oxygen evolution reaction. *J. Phys. Chem. C* **2017**, *121*, 6455-6463, doi:10.1021/acs.jpcc.6b12652.
8. Hussain, N.; Yang, W.; Dou, J.; Chen, Y.; Qian, Y.; Xu, L. Ultrathin mesoporous F-doped α-Ni(OH)2 nanosheets as an efficient electrode material for water splitting and supercapacitors. *J. Mater. Chem. A* **2019**, *7*, 9656-9664, doi:10.1039/C9TA01017C.
9. Mishra, S.; Daniele, S. Metal–organic derivatives with fluorinated ligands as precursors for inorganic nanomaterials. *Chem. Rev.* **2015**, *115*, 8379-8448, doi:10.1021/cr400637c.
10. Bekermann, D.; Barreca, D.; Gasparotto, A.; Maccato, C. Multi-component oxide nanosystems by Chemical Vapor Deposition and related routes: challenges and perspectives. *CrystEngComm* **2012**, *14*, 6347-6358, doi:10.1039/C2CE25624J.
11. Mishra, S.; Daniele, S. Molecular engineering of metal alkoxides for solution phase synthesis of high-tech metal oxide nanomaterials. *Chem. Eur. J.* **2020**, *26*, 9292-9303, doi:10.1002/chem.202000534.
12. Barreca, D.; Fois, E.; Gasparotto, A.; Maccato, C.; Oriani, M.; Tabacchi, G. The early steps of molecule-to-material conversion in chemical vapor deposition (CVD): a case study. *Molecules* **2021**, *26*, 1988, doi:10.3390/molecules26071988.
13. Klotzsche, M.; Barreca, D.; Bigiani, L.; Seraglia, R.; Gasparotto, A.; Vanin, L.; Jandl, C.; Pöthig, A.; Roverso, M.; Bogialli, S., et al. Facile preparation of a cobalt diamine diketonate adduct as a potential vapor phase precursor for Co_3O_4 films. *Dalton Trans.* **2021**, *50*, 10374-10385, doi:10.1039/D1DT01650D.
14. Barreca, D.; Bigiani, L.; Klotzsche, M.; Gasparotto, A.; Seraglia, R.; Jandl, C.; Pöthig, A.; Fois, E.; Vanin, L.; Tabacchi, G., et al. A versatile Fe(II) diketonate diamine adduct: preparation, characterization and validation in the chemical vapor deposition of iron oxide nanomaterials. *Mater. Chem. Phys.* **2022**, *277*, 125534, doi:10.1016/j.matchemphys.2021.125534.
15. Stienen, C.; Grahl, J.; Wölper, C.; Schulz, S.; Bendt, G. Fluorinated β-diketonate complexes M(tfac)$_2$(TMEDA) (M = Fe, Ni, Cu, Zn) as precursors for the MOCVD growth of metal and metal oxide thin films. *RSC Adv.* **2022**, *12*, 22974-22983, doi:10.1039/D2RA01338J.
16. Utke, I.; Swiderek, P.; Höflich, K.; Madajska, K.; Jurczyk, J.; Martinović, P.; Szymańska, I.B. Coordination and organometallic precursors of group 10 and 11: focused electron beam induced deposition of metals and insight gained from chemical vapour deposition, atomic layer deposition, and fundamental surface and gas phase studies. *Coord. Chem. Rev.* **2022**, *458*, 213851, doi:10.1016/j.ccr.2021.213851.

17. Utriainen, M.; Kröger-Laukkanen, M.; Johansson, L.-S.; Niinistö, L. Studies of metallic thin film growth in an atomic layer epitaxy reactor using M(acac)$_2$ (M=Ni, Cu, Pt) precursors. *Appl. Surf. Sci.* **2000**, *157*, 151-158, doi:10.1016/S0169-4332(99)00562-0.
18. Lindahl, E.; Ottosson, M.; Carlsson, J.-O. Atomic layer deposition of NiO by the Ni(thd)$_2$/H$_2$O precursor combination. *Chem. Vap. Deposition* **2009**, *15*, 186-191, doi:10.1002/cvde.200906762.
19. Lindahl, E.; Lu, J.; Ottosson, M.; Carlsson, J.O. Epitaxial NiO (100) and NiO (111) films grown by atomic layer deposition. *J. Cryst. Growth* **2009**, *311*, 4082-4088, doi:10.1016/j.jcrysgro.2009.06.030.
20. Utriainen, M.; Kröger-Laukkanen, M.; Niinistö, L. Studies of NiO thin film formation by atomic layer epitaxy. *Mater. Sci. Eng., B* **1998**, *54*, 98-103, doi:10.1016/S0921-5107(98)00135-4.
21. Chandrakala, M.; Raj Bharath, S.; Maiyalagan, T.; Arockiasamy, S. Synthesis, crystal structure and vapour pressure studies of novel nickel complex as precursor for NiO coating by metalorganic chemical vapour deposition technique. *Mater. Chem. Phys.* **2017**, *201*, 344-353, doi:10.1016/j.matchemphys.2017.08.056.
22. Emmenegger, F.; Schlaepfer, C.W.; Stoeckli-Evans, H.; Piccand, M.; Piekarski, H. Chelate effect in the gas phase. The complexes of Ni(2,2,6,6-tetramethyl-3,5-heptanedionate)$_2$ with bidentate ligands. *Inorg. Chem.* **2001**, *40*, 3884-3888, doi:10.1021/ic0014540.
23. Maccato, C.; Bigiani, L.; Carraro, G.; Gasparotto, A.; Seraglia, R.; Kim, J.; Devi, A.; Tabacchi, G.; Fois, E.; Pace, G., et al. Molecular engineering of Mn^{II} diamine diketonate precursors for the vapor deposition of manganese oxide nanostructures. *Chem. Eur. J.* **2017**, *23*, 17954-17963, doi:10.1002/chem.201703423.
24. Barreca, D.; Carraro, G.; Devi, A.; Fois, E.; Gasparotto, A.; Seraglia, R.; Maccato, C.; Sada, C.; Tabacchi, G.; Tondello, E., et al. *b*-Fe$_2$O$_3$ nanomaterials from an iron(II) diketonate-diamine complex: a study from molecular precursor to growth process. *Dalton Trans.* **2012**, *41*, 149-155, doi:10.1039/C1DT11342A.
25. Barreca, D.; Carraro, G.; Gasparotto, A.; Maccato, C.; Seraglia, R.; Tabacchi, G. An iron(II) diamine diketonate molecular complex: synthesis, characterization and application in the CVD of Fe$_2$O$_3$ thin films. *Inorg. Chim. Acta* **2012**, *380*, 161-166, doi:10.1016/j.ica.2011.10.036.
26. Bandoli, G.; Barreca, D.; Gasparotto, A.; Maccato, C.; Seraglia, R.; Tondello, E.; Devi, A.; Fischer, R.A.; Winter, M. A cobalt(II) hexafluoroacetylacetonate ethylenediamine complex as a CVD molecular source of cobalt oxide nanostructures. *Inorg. Chem.* **2009**, *48*, 82-89, doi:10.1021/ic801212v.
27. Gasparotto, A.; Barreca, D.; Devi, A.; Fischer, R.A.; Fois, E.; Gamba, A.; Maccato, C.; Seraglia, R.; Tabacchi, G.; Tondello, E. Innovative M(hfa)$_2$•TMEDA (M=Cu, Co) precursors for the CVD of copper-cobalt Oxides: an integrated theoretical and experimental approach. *ECS Trans.* **2009**, *25*, 549-556, doi:10.1149/1.3207638.
28. Bandoli, G.; Barreca, D.; Gasparotto, A.; Seraglia, R.; Tondello, E.; Devi, A.; Fischer, R.A.; Winter, M.; Fois, E.; Gamba, A., et al. An integrated experimental and theoretical investigation on Cu(hfa)$_2$•TMEDA: structure, bonding and reactivity. *Phys. Chem. Chem. Phys.* **2009**, *11*, 5998-6007, doi:10.1039/b904145a.
29. Fois, E.; Tabacchi, G.; Barreca, D.; Gasparotto, A.; Tondello, E. "Hot" surface activation of molecular complexes: insight from modeling studies. *Angew. Chem. Int. Ed.* **2010**, *49*, 1944-1948, doi:10.1002/anie.200907312.
30. Barreca, D.; Fois, E.; Gasparotto, A.; Seraglia, R.; Tondello, E.; Tabacchi, G. How does Cu^{II} convert into Cu^{I}? An unexpected ring-mediated single-electron reduction. *Chem. Eur. J.* **2011**, *17*, 10864-10870, doi:10.1002/chem.201101551.
31. Tabacchi, G.; Fois, E.; Barreca, D.; Gasparotto, A. CVD precursors for transition metal oxide nanostructures: molecular properties, surface behavior and temperature effects. *Phys. Status Solidi A* **2014**, *211*, 251-259, doi:10.1002/pssa.201330085.
32. Benedet, M.; Barreca, D.; Fois, E.; Seraglia, R.; Tabacchi, G.; Roverso, M.; Pagot, G.; Invernizzi, C.; Gasparotto, A.; Heidecker, A.A., et al. Interplay between coordination sphere engineering and properties of nickel diketonate–diamine complexes as vapor phase precursors for the growth of NiO thin films. *Dalton Trans.* **2023**, *52*, 10677-10688, doi:10.1039/D3DT01282D.
33. Benedet, M.; Maccato, C.; Pagot, G.; Invernizzi, C.; Sada, C.; Di Noto, V.; Rizzi, G.A.; Fois, E.; Tabacchi, G.; Barreca, D. Growth of NiO thin films in the presence of water vapor: insights from experiments and theory. *J. Phys. Chem. C* **2023**, 10.1021/acs.jpcc.3c05067, doi:10.1021/acs.jpcc.3c05067.
34. Kruve, A.; Kaupmees, K.; Liigand, J.; Oss, M.; Leito, I. Sodium adduct formation efficiency in ESI source. *J. Mass Spectrom.* **2013**, *48*, 695-702, doi:10.1002/jms.3218.
35. Zhao, Y.; Truhlar, D.G. The M06 suite of density functionals for main group thermochemistry, thermochemical kinetics, noncovalent interactions, excited states, and transition elements: two new

functionals and systematic testing of four M06-class functionals and 12 other functionals. *Theor. Chem. Account* **2008**, *120*, 215-241, doi:10.1007/s00214-007-0310-x.

36. Frisch, M.J.; Trucks, G.W.; Schlegel, H.B.; Scuseria, G.E.; Robb, M.A.; Cheeseman, J.R.; Scalmani, G.; Barone, V.; Mennucci, B.; Petersson, G.A.; et al. *Gaussian 09*, *Revision D.02*; Gaussian, Inc.: Wallingford, CT, USA, 2009.
37. Martin, J.M.L.; Sundermann, A. Correlation consistent valence basis sets for use with the Stuttgart–Dresden–Bonn relativistic effective core potentials: the atoms Ga–Kr and In–Xe. *J. Chem. Phys.* **2001**, *114*, 3408-3420, doi:10.1063/1.1337864.
38. Dunning Jr., T.H.; Hay, P.J.; in. *Modern Theoretical Chemistry*; Vol. 3, pp. 1-28, Plenum: New York, 1977.
39. Reed, A.E.; Weinhold, F. Natural localized molecular orbitals. *J. Chem. Phys.* **1985**, *83*, 1736-1740, doi:10.1063/1.449360.
40. Bader, R.F.W. A quantum theory of molecular structure and its applications. *Chem. Rev.* **1991**, *91*, 893-928, doi:10.1021/cr00005a013.
41. Tang, W.; Sanville, E.; Henkelman, G. A grid-based Bader analysis algorithm without lattice bias. *J. Phys. Condens. Matter* **2009**, *21*, 084204, doi:10.1088/0953-8984/21/8/084204.